Applied Catalysis B: Environment and Energy 353 (2024) 124057

Contents lists available at ScienceDirect

Applied Catalysis B: Environment and Energy

journal homepage: www.elsevier.com/locate/apcatb

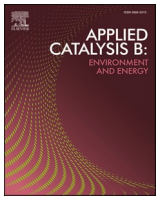

Enhanced pizeopotential-mediated catalytic oxidation mechanism of formaldehyde and anti-deactivation performance onto ZnO surface

Weina Zhao [a,b], Gu Wang [a,b], Shengnan Song [a,b], Meicheng Wen [a,b], Guiying Li [a,b], Taicheng An [a,b,*]

[a] Guangdong-Hong Kong-Macao Joint Laboratory for Contaminants Exposure and Health, Guangdong Key Laboratory of Environmental Catalysis and Health Risk Control, Institute of Environmental Health and Pollution Control, Guangdong University of Technology, Guangzhou 510006, China
[b] Guangzhou Key Laboratory of Environmental Catalysis and Pollution Control, Guangdong Technology Research Center for Photocatalytic Technology Integration and Equipment Engineering, School of Environmental Science and Engineering, Guangdong University of Technology, Guangzhou 510006, China

ARTICLE INFO

Keywords:
Formaldehyde oxidation
Piezoelectric catalysis
Catalytic oxidation
DFT calculations

ABSTRACT

Effective formaldehyde catalytic oxidation at mild conditions to satisfy stringent environmental regulations is urgently required for conquering hazardous threats to ambient air and human health. The utilization of piezoelectric polarization induced by mechanical strain has emerged as a highly effective strategy for environmental remediation, tremendously promoting catalytic oxidation processes. Herein, first principles calculations integrated with piezoelectric model were utilized to explore formaldehyde oxidation on ZnO(100). The underlying quantitative relationship between adsorption capacity and external strain ratios was revealed, with a −12 % deformation ratio leading to optimal adsorption. Unexpectedly, the free energy barrier of rate determining step is significantly reduced in piezocatalytic system. Interestingly, ZnO under external compression not only exhibit effectively enhanced piezopotential activity, but also resolved the catalyst deactivation problem by removing CO_2 and H_2O from surface. This work highlights the role of piezopotential in VOCs catalytic oxidation, and suggests a strategy for designing piezoelectric catalysts.

1. Introduction

With the rapid improvement of global industry and living standards, human society is facing a series of serious ambient air pollution due to the release of hazardous substances into the ecosystem [1,2]. Formaldehyde (HCHO), emitted from widely used artificial materials and household products, is the most dominant and pernicious indoor air pollutant with the characteristics of colorless and strong pungent smells. Long-term exposure to HCHO, over a 0.08 mg/m^3 limit of indoor air by China's standards [3], may cause severe and hazardous threats to human health leading to discomfort, headache, eye and respiratory irritation, fatigue, dullness and even cancer [4,5]. Meanwhile, being the smallest and most abundant aldehyde, HCHO can be utilized as a model pollutant to explore novel technologies for volatile organic compound (VOC) treatment. Therefore, great efforts endowed to effectively remove HCHO at room temperature for satisfying stringent environmental regulations is urgently required from both fundamental and practical points of view.

Among various HCHO removal options, adsorption and catalytic oxidation are considered as two promising candidates for effective HCHO removal [4,6–8]. Adsorption technology is a hot research topic, but even with surface modification or combination as composite materials, the capacity of the adsorbent for VOCs collection is still unsatisfactory. Catalytic oxidation technology under mild conditions appears to be one of the most effective strategies to reduce HCHO content from industrial waste streams [9,10], due to high economic feasibility, low generation rate of secondary pollutants and controllable selectivity of products operated at lower temperatures. For example, Chen et al. synthesized palladium-containing CeO_2 catalysts with different morphologies by a simple hydrothermal method, and found that HCHO could be converted into H_2O and CO_2 at room temperature with high efficiency and good stability [11]. Yu et al. studied the activity and stability of Au/-Al_2O_3 at room temperature by revealing the strong metal support interaction between Au nanoparticles and irreducible γ-Al_2O_3 supports, and the results showed that the rate-limiting step in oxidation of formaldehyde (i.e., the oxidation of formate intermediates) is

* Corresponding author at: Guangdong-Hong Kong-Macao Joint Laboratory for Contaminants Exposure and Health, Guangdong Key Laboratory of Environmental Catalysis and Health Risk Control, Institute of Environmental Health and Pollution Control, Guangdong University of Technology, Guangzhou 510006, China.
E-mail address: antc99@gdut.edu.cn (T. An).

https://doi.org/10.1016/j.apcatb.2024.124057
Received 16 February 2024; Received in revised form 1 April 2024; Accepted 7 April 2024
Available online 9 April 2024
0926-3373/© 2024 Elsevier B.V. All rights reserved.

enhanced by adding gold nanoparticles [12]. Similarly, Qin et al. prepared Ru/CeO_2 and Ru/Al_2O_3 catalysts by immersion method, and found that the Ru/CeO_2 catalysts exhibit excellent catalytic performance with HCHO all converted at about 90℃ [13]. Despite catalytic oxidation technology has the potential of continuous and thorough oxidation of gaseous HCHO, unfortunately it still suffers from that the catalysts with high room temperature of formaldehyde oxidation activity usually involve the scarce resources of noble metals and are easy to be deactivated [14–16]. Many researchers are thus widely devoted to combine traditional HCHO catalytic oxidation with new technologies.

Piezoelectric catalysis has currently brought"light" to environmental remediation induced by ubiquitous mechanical strain, including pressure, stir, ultrasound, waterfall, and wind [17–22]. The piezoelectric phenomenon is firstly observed via Curie brothers in 1880 when applying mechanical force to nanomaterials [23,24]. Under mechanical stress by squeezing or stretching, the atoms in catalysts are displaced from their original position yielding the collective induced polarization of charges in the whole crystal and hence a piezoelectric potential (piezopotential) is generated while net positive and negative charges migrate to the opposite and outer faces of the catalyst to trigger redox reactions [25]. The piezoelectricity origins from the non-centrosymmetric nature of the material yielding in-built electric field in materials, while it returns to an uncharged equilibrium state when there is no external strain. Recently, non-centrosymmetric metal oxides (e.g., ZnO [26–28], $BiFeO_3$ [29,30], $BaTiO_3$ [31,32], SnO_2 [33]) and metal disulfides [34–36] (WS_2, MoS_2 and WSe_2) have attracted people's attention as ideal alternatives for piezoelectric catalytic degradation of VOCs.

The typical hexagonal wurtzite ZnO has been regarded as a highly promising and efficient piezoelectric material for elimination of VOCs because of the high piezoelectric output, stability and environmental friendliness [37]. Recently, extensive studies have been carried out on the role of in-built piezoelectric field in promoting the catalytic efficiency of ZnO via charge separation within the material [38–40]. Compared with other oxidation technologies, piezoelectric catalysis is more energy-efficient because no matter the origin (mechanically or spontaneously), the in-built electric field can be generated which affects the redox reactions occurring on materials surfaces [41,42]. For example, ZnO surface can induce the formation of hydroxyl radicals and reactive superoxide radicals under sonication, thereby accelerating and enhancing the oxidation properties of Ibuprofen molecules [43]. The nanocomposite ZnO-GO undergoes deformation under ultrasonic vibration while an internal polarization potential is generated to promote the separation and migration of free electricity, thereby enhancing methylene blue degradation [44]. A twin-brush ZnO piezoelectric mesocrystal (TB-ZnO) with rich oxygen vacancies was fabricated by Peng et al. [45] to optimize piezo-polarization charge migration and provide abundant active sites, and both experimental and theoretical results showed ultra-high activity for PMS activation in the ibuprofen degradation. Obviously, piezoelectric catalysis plays a pivotal role in energy conversion and environmental restoration. Yet, most of the abovementioned piezoelectric catalysis solely concentrate on the modification of catalytic materials, while how to overcome the main bottlenecks in piezocatalysis is an intriguing problem that puzzles people, facing the material defects of low sensitivity to strain, insufficient active sites and elusive piezoelectric catalytic mechanism during pollutant degradation [46]. Therefore, a theory to clear the roles of the sensitivity of piezoelectric catalyst to strain, active sites and anti-deactivation performance in relation to catalytic oxidation mechanism of HCHO is thus urgently required.

In this work, the first-principles theoretical analysis on the piezoelectric catalytic mechanism and anti-deactivation performance for HCHO oxidation onto ZnO were reported. Large-scale calculations based on DFT integrated with a periodic continuum model are utilized for modeling the degradation process at the solid–gas interface. The specific piezoelectric catalytic oxidation mechanism, the sensitivity of ZnO surface to strain, the anti-deactivation performance and the reaction pathways of HCHO catalytic oxidation were confirmed via the calculations of the adsorption energies, the electronic structure distribution, charge density difference, deformation density, transition state theory, etc. This work not only might guide the design of high-efficiency environmentally friendly piezoelectric catalysts for oxidation of formaldehyde, but also prolongs the application of piezoelectric materials in the field of VOCs catalytic oxidation.

2. Methodology and calculation details

In this study, all density functional theory (DFT) modeling is performed using the Vienna ab initio simulation package (VASP). Electron exchange-correlation is described with the Perdew-Burke-Ernzerhof functional using the generalised gradient approximation (GGA) [47], with a cutoff energy of 400 eV for the planewaves. In the simulation, a slab model of 4×2super cells with five ZnO layers is used with the optimized lattice parameters of (a = 13.04 Å, b = 10.44 Å and c = 25.00 Å), and a ~13 Å vacuum layer is utilized to minimize layer-to-layer interactions. The unit cell of ZnO bulk was optimized with a Monkhorst-Pack k-point grid of 5×5×3, while only the G-point was utilized for ZnO surfaces due to the large unit cell. The conjugate gradient method was used for geometry optimization with a convergence threshold set at 0.02 eV/Å for the force on each atom. In addition, HSE06 hybrid functional [48] is used to obtain the accurate density of state (DOS). In all calculations, the gas molecules and the top two layers of ZnO(100) are relaxed while the bottom three layers are fixed. For the Bader charge analysis [49], a positive value of Δρ indicates the transfer of electrons from ZnO substrate to gas molecules and vice versa.

For reactants, intermediates and products, various adsorption models were calculated to determine their favorable adsorption sites. The correction of Gibbs free energy (G(T)) was calculated using vaspkit [50] with an input temperature of 298.15 K. The adsorption energy (E_{ads}) and Gibbs free energy are defined by the following equations:

$$E_{ads} = E_{total} - E_{slab} - E_{adsorbate}$$

$$G(\mathrm{T}) = E + ZPE + \Delta G_{0\to T}$$

Where E_{total} is the total energy of the slab with adsorbable, E_{slab} is the energy of the surface slab, $E_{adsorbate}$ is the energy of the adsorbent in the gaseous phase. E is the reaction energy related to the reactant and product molecules adsorbed on the catalytic surface in each reaction step, ZPE is zero-point vibration energy correction, $\Delta G_{0\to T}$ is interal Gibbs free energy difference between 0 K and T K (T = 298.15 K). All transition state structures were searched via the climbing-image nudged elastic band (CI-NEB) method [51] and subsequently a vibrational analysis was used to validate the identified transition states by a single imaginary frequency mode. The reaction energy barrier (E_b) and reaction energy (ΔE) are defined by the following equations:

$$E_b = E_{TS} - E_{IS}$$

$$\Delta E = E_{FS} - E_{IS}$$

Where, E_{IS}, E_{TS}, and E_{FS} are the energy of the initial, transitional, and final states, respectively. The positive and negative ΔE values indicate endothermic and exothermic reactions, respectively.

3. Results and discussion

3.1. Theoretical implementation of piezoelectric polarization model

For piezoelectric catalytic system, the atomic structure of catalyst is extremely critical due to that piezoelectric effect is sensitive to structure deformation. Hence, wurtzite structure of ZnO with a space group of P63mc is used in this study, which is also the most stable crystal phase under natural conditions. The DFT optimized lattice parameters of ZnO

unit are ($a = b = 3.26$ Å and $c = 5.22$ Å), which is in good agreement with the previous calculated results and experimental lattice (Table 1). Fig. 1a shows the crystal structure of wurtzite ZnO, where purple and red sphere indicates Zn and O atom, respectively. The wurtzite ZnO unit is a regular tetrahedron structure while the zinc atom is located near the center of oxygen tetrahedron structure. The distance between the central zinc atom and adjacent four oxygen atoms is different with the distance of Zn-O bond along (001) direction longer, indicating that off-centering displacement of zinc cation within oxygen tetrahedron will yield spontaneous polarization in such direction (Fig. 1b). Many previous studies have also shown that there is an admirable spontaneous polarization within wurtzite ZnO unit along (001) axis. Massidda et al. obtained spontaneous polarization value of -0.047 C/m^2 by a *GW* theoretical scheme. In addition, an experimental model based on nonlinear optics also gives an estimate value of spontaneous polarization of -0.07 ± 0.02 C/m^2 [52]. This suggests that deformations in this direction will induce a potential difference. Therefore, the variation of bond length with various strain ratio in *c*-axis was focused, and the unstrained bond length of Zn-O(top) and Zn-O(bottom) in ZnO unit were 1.99 and 1.98 Å, respectively. When subjected to an external force strain, the center of charge shifts, resulting in piezoelectric polarization. As shown in Fig. 1c, there is obvious offset of the charge center due to the subjected strain while blue and white indicate the polarized and original negative charge center, respectively.

The polarization direction is thus identified along *c*-axis in ZnO unit, indicating that shift of Zn ion would affect polarization intensity. Fig. 1d presents the variation trend of Zn-O_{top} bonding length ($d_{Zn\text{-}O}$) in ZnO unit regarding the deformation ratio where strain range is evaluated by the sum of radii of Zn and O ions [53]. It is found that $d_{Zn\text{-}O}$ gradually decreases as the compressive strain ratio increases, while it shows a slight increase when the compression increases to -12 %. Conversely, the increase in tension will elongate $d_{Zn\text{-}O}$, resulting in shift of Zn atom away from the central site along polarization direction. In addition, the offset distance of the central Zn atom from lattice midline along the polarization direction were also examined. Note that the greater the distance, the greater the polarization intensity [54]. Fig. 1e shows that the offset distance of the central Zn atom exhibits gradual increase with the increase of the tension strain, while it shows a rapid increase as the compressive strain ratio increasing. Obviously, the piezoelectric polarization effect exists both under tensile strain and compressive strain, but with that under compressive strain is more obvious.

To clarify the effect of structure strain on the catalytic oxidation activity of HCHO, ZnO(100) surface as the reaction interfacial planes was selected since such crystallography plane dominate piezoelectric polarization orientation [55] (Table S1). For example, the O(top) atom in bulk would move along (00$\bar{1}$) direction under compressive strain, and thus three coordination oxygen atoms onto ZnO(100) surface as shown in Fig. 2a will move upward which makes it easier to participate in piezoelectric reactions. Figs. 2a and b shows the side and top views of ZnO(100) surface model, respectively. ZnO(100) surface is modeled by a rectangular unit cell of five ZnO layer slabs with lattice parameters of (13.04 Å, 10.44 Å, 160 atoms), and vacuum spacing is usually larger than 10 Å. The surface exhibits high symmetry with five possible adsorption sites, namely top O (T_O), top Zn (T_{Zn}), hollow position (H), bridge site of Zn and adjacent O atoms(B_1) and bridge site of top two adjacent Zn atoms (B_2) (Fig. 2b). When uniaxial compressive strain with -12 % is applied, the optimized lattice parameters of ZnO(100) is (13.04 Å, 9.19 Å, 160 atoms) while the side and top structure is shown in Fig. S1. With respect to original static surface, buckling height (ΔH) of compressive surface showed a slight increase by 0.31 Å, while two surface Zn-O bond length also increase from 1.87 Å(top), 2.00 Å(bottom) to 1.94 Å,2.02 Å, respectively. From changes in surface structures, the compressive surface has undergone a certain degree of deformation which can yield internal polarization electric fields, but still maintains a graphite honeycomb structure just like the original static structure.

Table 1
Structural parameters (Å) of bulk wurtzite ZnO.

Structural parameters (Å)		
a	*c*	/
3.25	5.21	Ref. [56]
3.27(+0.62 %)	5.25(+0.77 %)	Ref. [57]
3.26(+0.31 %)	5.22(+0.19 %)	This work

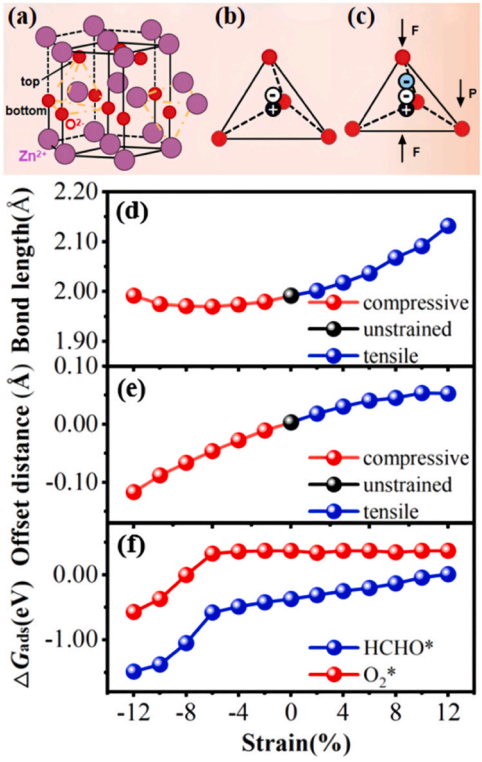

Fig. 1. (a) Crystal structure of wurtzite-type ZnO bulk (color scheme: Purple-Zn; red-O); Charge distribution of ZnO bulk (b) before stress and (c) after stress, black is the positive charge center, white is negative charge center and blue is negative charge center after stress; (d) The bond length of Zn-O_{top} varies with the strain ratio; (e) the offset distance of the central Zn atom; and (f) The variation of adsorption free energies of HCHO and O_2 with different strain ratios.

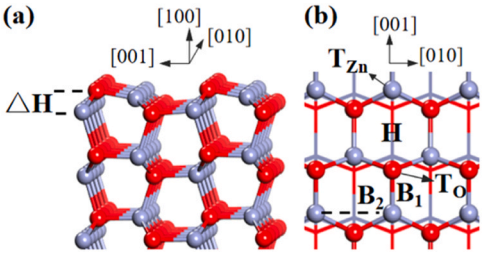

Fig. 2. (a) Side and (b) top views of ZnO(100) surface. (color scheme: Blue-gray-Zn; red-O; the same below). The coordinates are the crystal plane index.

3.2. *The adsorbed species and their relative electronic structures onto ZnO surfaces*

To clear the mechanism and kinetics of catalytic oxidation of HCHO, the adsorption behavior involving reactive species as the key first step is explored where elucidates the microscopic interaction between reactants and interfaces. Herein, the behavior of HCHO and O_2 onto Zn

(100) surface were firstly quantified and compared their relative sensitivity to different degrees of piezoelectric polarization.

As depicted in Fig. 1f, the tensile strain results in a slight decrease in adsorption energy of HCHO molecules onto the ZnO(100) surface, aligning with observed shift in atomic positions. This shift elongates Zn-O_{top} bond within bulk structure, prompting surface atoms to move towards ($\bar{1}$00) direction. Consequently, this movement hinders the interaction between adsorbed molecule and reactive surface. Nevertheless, oxygen molecules still remain unabsorbed states under tensile strain. Conversely, during the compressive strain process, the adsorption energy of both HCHO and O_2 molecules exhibits a gradual increase, likely due to the movement of surface atoms onto ZnO(100) in (100) direction. The parallel trends observed suggest a potential correlation between adsorption energy and bond length. The relationship between adsorption energy and compressive strength was observed to be positively correlated, with a maximum adsorption energy of −1.49 eV at a compressive strain of 12 %. Consequently, adsorption energies of HCHO and O_2 were found to be significantly influenced by the structural strain of ZnO within a specific range of compressive strain. Therefore, the research onto ZnO(100) surface with a compressive strain of 12 % was focused in the following study.

3.2.1. HCHO adsorption onto ZnO surfaces

For HCHO adsorption, many possible initial geometrical structures were first calculated and the most favorable adsorption configuration onto ZnO(100) surface is shown in Figs. 3a and b. As shown, HCHO adsorbs parallelly onto hollow site through a surface three-coordinated Zn (Zn_{3c}) and three-coordinated O (O_{3c}) site via its O/C end forming a O-Zn (1.93 Å) and C-O (1.56 Å) bond, respectively. The adsorption results in an increase of C═O bond in HCHO from 1.22 Å (in the isolated state) to 1.33 Å and also a decrease of surface Zn-O atom distance bonded to HCHO molecule onto ZnO surface from 3.40 to 3.21 Å. Similarly, onto the piezo-polarized ZnO(100) surface by −12 %, HCHO also adsorbs in a molecular plane parallel to the surface and the adsorption configurations are shown in Fig. S2. With respect to that onto 0 % ZnO(100), the bonding distance between O atom in HCHO* and surface Zn_{3c} atom is shortened to 1.91 Å, while the bonding distance between C atom in HCHO* and surface O_{3c} atom is shortened to 1.51 Å. For the adsorbed HCHO* molecule, the bonding distance of C═O bond is elongated to 1.36 Å, indicating the C═O bond being weakened by the polarized surface. Next, the adsorption free energy of HCHO onto ZnO(100) surface was calculated, which is defined by the formula $\Delta G_{ads} = G_{total} - G_{sur} - G_{adsorbate}$. In accordance with the trends of structural change, the adsorption free energy of HCHO onto −12 % ZnO(100) and 0 % ZnO (100) are obtained as −1.49 and −0.37 eV, respectively, suggesting that compressive strain would yield stronger interaction between HCHO and the surface.

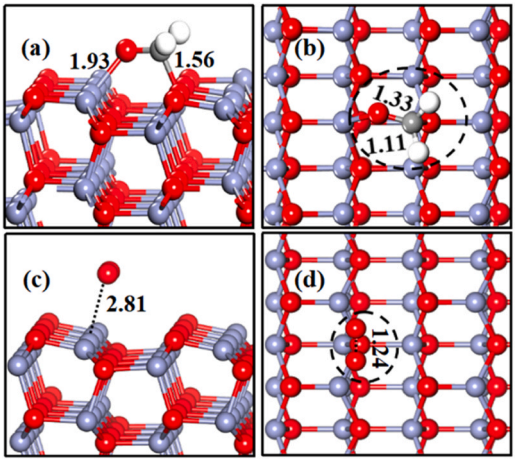

Fig. 3. A schematic illustration of side (a, c) and top (b, d) views of optimized configurations of HCHO and O_2 molecule adsorbed onto ZnO(100) surface. (color scheme: Grey-C; white-H the same below).

In Fig. 4a, the calculated total density of states (TDOS) of the adsorbed HCHO onto ZnO(100) surface with the strain of 0 % and −12 % were compared. Compared to that onto 0% ZnO(100), TDOS onto −12 % ZnO(100) moves downward to maintain a lower energy which is consist with the calculated adsorption free energy [58], whereas the rough shape is roughly constant. In addition, according to the further calculated projected DOS (PDOS) in Fig. 5, the E_f level of adsorbed system in the presence of −12 % is mainly contributed from HCHO molecule where perfectly overlap hybrid with the lattice surface O_{2p} and Zn_{3d} states, while the orbitals of HCHO onto 0 % ZnO(100) is ~0.3 eV lower than that of E_f level. This demonstrates that electron transfer from surface to the adsorbed HCHO molecules is more feasible onto −12 % ZnO(100) than onto 0 % ZnO(100).

To further explore the potential mechanisms of the variations in HCHO adsorption caused by subjected strain, Bader charge was calculated (Table 2). Note that a positive number Δρ indicates that the species obtain electrons. It illustrates that electrons are transferred from ZnO (100) surface to adsorbed HCHO molecules regardless of whether there is an external strain or not, while more electrons (0.04 |e|) are transferred onto −12 % ZnO(100) than without external forces. Such conclusion is consistent with above adsorption energy and also confirmed by following calculated charge density difference plots. Fig. 6a shows that charge distribution around HCHO molecules (the O and C atoms) generally indicate ionic O-Zn and C-O bonds onto ZnO surface. Unexpectedly, an obvious greater amount of charge is accumulated onto HCHO when the compressed ratio increases to −12 %, with ZnO surface showed a state of charge loss, consisted with the above electronic structure analysis and adsorption trend. These indicate that built-in electric field formed by piezoelectric effect would enhance adsorption behavior of reactive species.

3.2.2. O_2 adsorption onto ZnO surfaces

For O_2 adsorption, O_2 molecule also prefers to locate parallelly above the B_2 site with a straight-line distance of 2.81 Å between the surface plane (Fig. 3c and d). The calculated adsorption free energy of O_2 onto Zn(100) surface is 0.37 eV, indicating that oxygen adsorption process belongs to physisorption which is similar to the results of Pacchioni et al. [59]. Onto −12 % ZnO(100) surface, the adsorption free energy of O_2 shows a sharp enhance to −0.57 eV while the most stable adsorption configuration is basically the same as without polarization effect (Fig. S2). Meanwhile, the O═O bond length of O_2* is elongated to 1.30 Å (1.23 Å in gaseous phase), while the distance between O_2 and surface plane is decreased to 2.12 Å. This indicates the adsorbed O_2 molecule is activated by the piezoelectric polarization effect onto ZnO (100) surface, which would facilitate the subsequent reactions.

In Figs. 4b, 5c and d, the calculated total and projected density of states of the adsorbed O_2 onto ZnO(100) surface with the strain of 0 % and −12 % were shown. Compared to that onto 0 % ZnO(100), the compressive strain would shift the energy of the total adsorbed system towards more negative energy yielding greater adsorption energy, which can also be concluded by the number of DOS particles near Fermi energy level onto −12 % ZnO(100). Further, PDOS of O_2* molecule shifts significantly upwards with a new peak introduced across the Fermi energy level in Fig. 5d, consistent with Bader charge analysis where 0.38 |e| and 0.15 |e| electrons are transferred from −12 % and 0 % ZnO(100) surface to the adsorbed O_2* molecules in Table 1, respectively. To further evaluate the effect of compressive force on O_2 adsorption, the charge density difference plot is also calculated. As shown in Figs. 6c and d, no charge overlaps onto 0 % ZnO surface which may be attributed to weak physical adsorption of O_2, while more charges accumulate in the region where O_2 molecule bonds with −12 % ZnO(100) surface exhibiting a strong charge transfer from surface to O_2 molecule. This indicates that O_2 molecule has a stronger interaction with −12 % ZnO(100)

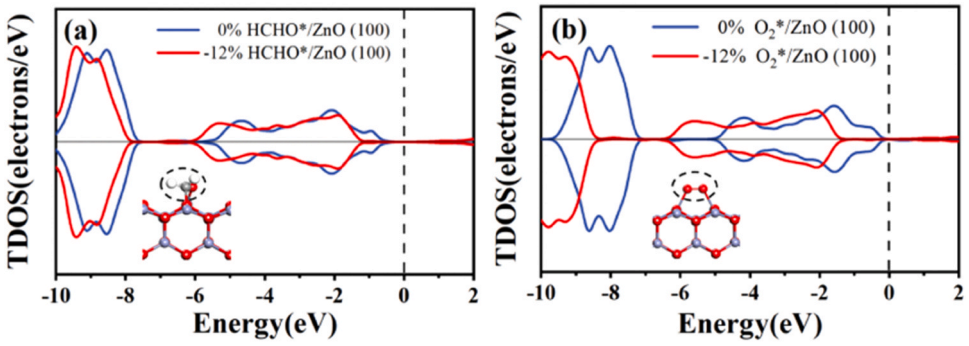

Fig. 4. The total density of states for adsorbed (a) HCHO and (b) O_2 onto 0 % ZnO(100) and −12 % ZnO(100). The Fermi level is shown by the black dashed lines, which is set to be zero (the same below).

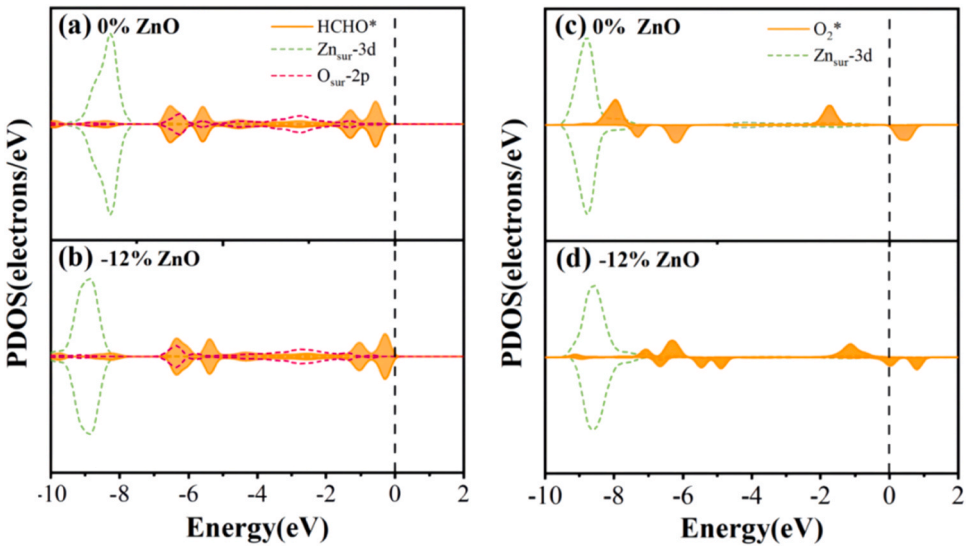

Fig. 5. The projected density of states for (a, b) HCHO and (c, d) O_2 adsorption onto 0 % and −12 % ZnO(100). HCHO* and O_2* are the adsorbed states, while Zn_{sur} and O_{sur} represent Zn and O atoms bonded with adsorbed molecules onto ZnO surface, respectively.

Table 2
The adsorption free energy (ΔG_{ads}/ΔG_{ads}',eV) and charge transfer quantity of HCHO (Δρ, |e|) and O_2 (Δρ', |e|) after adsorption onto 0 % and −12 % ZnO (100).

Type	0%		-12%	
	ΔG_{ads}	Δρ	ΔG_{ads}'	Δρ'
HCHO*	-0.37	0.40	-1.49	0.44
O_2*	0.37	0.15	-0.57	0.38

surface, which also corresponds to a greater adsorption energy.

3.3. The overall mechanism of catalytic oxidation of formaldehyde onto ZnO surfaces

For catalytic oxidation of HCHO, there are two possible pathways, i. e., the Eley-Rideal (ER) and Langmuir-Hinshelwood (LH) mechanism [60] which typically depends on the relative adsorption energy of O_2 and HCHO molecule. LH mechanism involves simultaneous chemisorption of all reactive species prior to catalytic activation before the reactions starts, while ER mechanism at least refers to O_2 in the gas phase which reacts directly with reactive species adsorbed at the catalytic site. As mentioned above, the adsorption free energy of HCHO is both greater than that of O_2 onto ZnO(100) surface with (-1.49 vs −0.57 eV) and without (-0.37 vs 0.37 eV) polarized compression force.

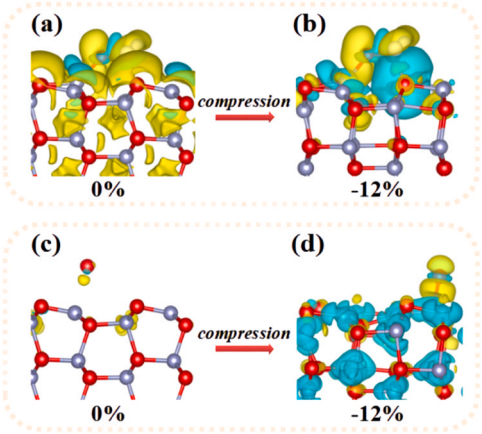

Fig. 6. Charge density difference plot for HCHO (a, b) and O_2 (c, d) adsorbed onto 0% ZnO(100) and - 12% ZnO(100) surface. Yellow and blue represent areas of electron accumulation or lack, respectively. The isosurface is set to 1.00 × 10^{-3} e/Å ^{3} (HCHO adsorption) and 2.00 × 10^{-3} e/Å ^{3} (O_2 adsorption).

This indicates that HCHO is preferentially adsorbed onto ZnO surface before O_2 to form a co-adsorption configuration. Therefore, in this work, we will systematically explore catalytic oxidation of HCHO with LH

mechanism onto both 0 % and −12 % ZnO(100) surface.

To understand the mechanism of catalytic oxidation process of HCHO through Langmuir Hinshelwood mechanism at the atomic scale, DFT calculations of the reaction free energies and important intermediate transition states of each step of HCHO oxidation onto ZnO(100) surface were performed (Fig. 7, S3 and S4). Four basic steps after co-adsorption of O_2 and HCHO are generally outlined as below:

$$HCHO^* + O_2^* \rightarrow {}^*CHO + {}^*OOH \quad (1)$$

$$^*CHO + {}^*OOH \rightarrow {}^*CHO + {}^*O + OH^* \quad (2)$$

$$^*CHO + {}^*O + {}^*OH \rightarrow HCO_2^* + {}^*OH \quad (3)$$

$$HCO_2^* + {}^*OH \rightarrow CO_2(g) + H_2O^* \quad (4)$$

3.3.1. *HCHO oxidation onto pristine ZnO(100) surface*

HCHO oxidation through LH mechanism onto ZnO(100) surface without piezoelectric catalytic effect was firstly studied. Considering many possible co-adsorption geometries, we finally obtained the most energetically favorable structure shown in Fig. S3, where HCHO and O_2 are adsorbed in molecular planes parallel to the surface plane with a calculated co-adsorption free energy of −0.07 eV onto ZnO(100) surface. The co-adsorption free energy is lower than the sum of individual adsorption energy of HCHO and O_2, which can be contributed to energy release induced by the bond formation of adsorbent and the adsorbed molecules. Such similar phenomenon was also reported in early study [61].

For the first H removal (step1: 1→TS1→2), an H atom of HCHO* is transferred to the nearby O_2* yielding *OOH species and *CHO. TS structure for the C-H bond breaking of HCHO is also searched showing that O_2* moves close to HCHO* forming C—H—O intermediate species with a distance of 1.14 and 1.99 Å, respectively. In step 1, the dissociation barrier is 0.20 eV with an exothermic energy of 1.55 eV, while the generated *CHO and *OOH is adsorbed onto the H and B_2 bridge site, respectively. The detailed transition state configuration in the reaction process is shown in Fig. S4. In step 2, O-O bond in *OOH species breaks, generating *OH species and *O species (2→TS2→3). This step requires overcoming a high free energy barrier of 1.29 eV with releasing energy of 0.45 eV, while the O-O bond length in TS2 is stretched from the initial 1.49–2.33 Å. Obviously, this step is not feasible kinetically at room temperature because of high free energy barrier. Subsequently (in step 3), the generated *O species in step 2 would combine with the *CHO species to generate the HCO_2* intermediate (3→TS3→4). Moreover, O* species and *CHO species in TS3 tend to move closer to each other which requires crossing a free energy barrier of 0.58 eV with an exothermic energy of 0.99 eV, while the distance of O*-Zn_{sur} (surface Zn atom) is elongated from 1.90 to 2.10 Å. We evaluated the migration of the generated OH* onto the surface to judge the subsequent participation in the reaction and found that there is almost no energy change during the OH* migration (4→4′). Then, in step 4, dehydrogenation of HCO_2* occurs while H atom isolated from HCO_2* combines with *OH species to produce H_2O* species and CO_2 molecules (4′→TS4→5). HCO_2* in TS4 is still adsorbed vertically onto the surface while the O-Zn_{sur} bond distance formed by HCO_2* and ZnO surface is elongated from 2.00 Å to 2.90 Å. This process requires crossing a free energy barrier of 0.76 eV with a large amount of exothermic energy of 2.46 eV.

Finally, the CO_2 molecule is desorbed from ZnO surface and H_2O* species has a tendency of moving close to the desorbed CO_2 molecule to form a H_2O molecule (5→FS) (Fig. S3). Note that this step is an endothermic process which requires a desorption energy of 1.20 eV. The results indicate that the formed final products, H_2O and CO_2 species are not easy to desorb from ZnO surface which will cause catalyst poisoning for long time. In addition, as can be seen from the above results, the rate-determining step of the entire HCHO oxidation onto ZnO(100) surface is O-O bond break process in *OOH with a high barrier of 1.29 eV (state TS2). This indicates that it is quite difficult to occur for HCHO oxidation onto pristine ZnO(100) surface.

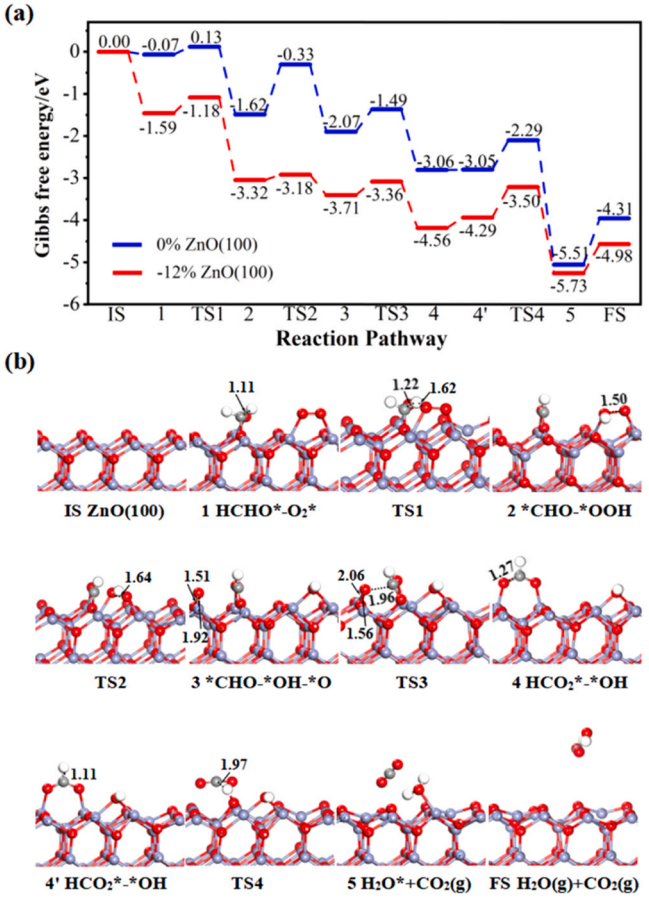

Fig. 7. (a) Free energy profiles for catalytic oxidation of HCHO onto ZnO(100) surfaces; (b) the calculated TS and intermediate state structures for catalytic oxidation of HCHO onto −12 % ZnO(100) surface.

3.3.2. *Catalytic oxidation of HCHO under piezoelectric catalytic effect*

To explore piezoelectric polarization effect on the reaction mechanism, DFT simulations of catalytic oxidation of HCHO onto ZnO model with a compressive strain of 12 % were proceeded. The co-adsorption structure with the most favorable energy was also calculated (Fig. 7b). Similar to that onto 0 % ZnO(100), HCHO oxidation begins with co-adsorption of HCHO and O_2 adsorbed in molecular planes parallel to the surface plane, while HCHO is preferentially adsorbed followed by O_2 adsorption onto −12 % ZnO(100). The co-adsorption free energy (-1.59 eV) is smaller than the sum of the individual adsorption energy of HCHO (-1.49 eV) or O_2 (-0.57 eV) in piezoelectric catalytic system, demonstrating that there is a strong interaction exists between surface and the adsorbent. Understandably, co-adsorption may induce structure deformation of absorbed molecules and the adsorbent, which requires energy consumption and also found for the pristine surface.

The elementary steps of catalytic oxidation of HCHO onto −12 % ZnO(100) surface is similar to that onto pristine surface but with different reaction energies in piezoelectric catalytic system. In the first dehydrogenation, an H atom of HCHO* is also transferred to the nearby O_2* group yielding *OOH and *CHO species (1→TS1→2), which requires crossing a free energy barrier of 0.41 eV by releasing an energy of 1.73 eV. In TS1 structure, the C-H bond length is elongated from 1.11 Å to 1.22 Å, while the distance of H—O_2* is 1.62 Å. The generated *CHO and *OOH group is adsorbed onto the H and B_2 bridge site, respectively. In the second step (2→TS2→3), compared to that onto pristine ZnO surface (1.29 eV), the barrier of O-O bond break onto −12 % ZnO(100)

is significantly reduced to 0.14 eV with the bond length elongated from 1.50 to 1.64 Å, indicating that the piezoelectric polarization greatly reduces the barrier of rate-determining step for the entire HCHO oxidation. Particularly, wurtzite ZnO has advantages in practical application for piezoelectric catalytic degradation of VOCs because it is environmentally friendly piezoelectric materials. The generated *OH is adsorbed on the B_2 bridge site while the *O group is adsorbed onto the H site. Subsequently, the *O species would combine with the *CHO species generated in the first step to yield HCO_2* intermediate vertically adsorbed onto the surface (3→TS3→4). In addition, O* species and *CHO species adsorbed onto the H hollow site in TS3 also tend to move closer to each other overcoming a free energy barrier of 0.35 eV with an exothermic energy of 0.85 eV, while the distance of O*—*CHO, O*-Zn_{sur} and O*-O_{sur} (surface O atom) is 1.96, 2.06, and 1.56 Å, respectively. Different from that onto pure surface, OH* species migrate towards HCO_2* species onto −12 % ZnO(100) surface (4→4′) requires overcoming a thermodynamic migration energy of ~0.27 eV which is feasible for a real reaction. This was accompanied by reacting with H atom detached from HCO_2* to produce H_2O* species and CO_2 molecule (4′→TS4→5). In TS4 structure, the C-H bond in HCO_2* is broken while the bond distance changes from 1.11 Å to 1.97 Å, resulting in a distance between CO_2 and surface of 2.15 Å. This process proceeds with a free energy barrier of 0.79 eV with an exothermic energy of 1.44 eV, indicating that dehydrogenation of HCO_2* becomes the rate determining step induced by the piezoelectric polarization effect. Finally, CO_2 desorption begins at the surface followed by H_2O* group getting close to the desorbed CO_2 molecule to yield H_2O molecule with an endothermic process of 0.75 eV, which ensures the catalytic oxidation of HCHO occurring after desorption to avoid catalyst poisoning induced via adsorbed product species during regeneration.

To better verify the desorption behavior of the yielded CO_2 and H_2O molecules under ambient conditions in this piezoelectric catalytic system, the desorption time (τ) was straight forwardly implemented according to the following formula [62]:

$$\tau = \frac{1}{Ae^{\frac{-E_{des}}{k_B T}}}$$

Where, k_B is the Boltzmann constant (8.63×10^{-5} eV /K). A is the bond vibration frequency (10^{12} Hz). T is room temperature (298.15 K). The detailed free energy barrier G_{bar} (eV) and Gibbs free energy change ΔG (eV) of each step of LH mechanism onto 0 % and −12 % ZnO(100) surface is shown in Table S2. The calculated desorption time of CO_2 and H_2O molecules onto 0 % and −12 % ZnO(100) surface was 1.80×10^8 s and 4.56 s, respectively. The results show that CO_2 and H_2O molecules is not easily desorbed from pristine surface, but would easily desorb from piezo-polarized ZnO(100) surface in piezoelectric catalytic system which is beneficial to avoid the inactivation of catalytic active sites and facilitate following reaction pathway in Fig. 7.

Our results show that piezoelectric polarization induced by external force can greatly reduce the free energy barrier and alter the rate-determining step of HCHO oxidation by LH mechanism in piezopotentail catalytic system. To demonstrate the pizeopotential-mediated catalytic performance, we did an experiment of HCHO catalytic oxidation on ZnO and compared the catalytic performance of ZnO under ultrasonic vibration or not. The results indicates that ZnO showed poor catalytic performance without the ultrasonic vibration, which is consist with a previous study reporting that pristine ZnO has no significant removal effect on HCHO oxidation at room temperature [63]. Inspiringly, the catalytic oxidation performance of ZnO was greatly improved under the ultrasonic treatment, with the conversion rate of HCHO increased by more than two times after ultrasonic treatment for 50 min (details in the supporting information). Our results agree with the conventional viewpoint that the piezoelectric polarization can improve the degradation activity of organic pollutants. Furthermore, the piezo-polarized ZnO (100) surface can be conducive to the desorption of CO_2 and H_2O molecules, avoiding the deactivation of catalytic active sites and facilitating the following reaction.

It is thus natural to ask what causes piezoelectric polarization induced by external force for the increase of HCHO oxidation activity in piezopotentail catalytic system. To illustrate the piezoelectric polarization in real space, we have constructed a charge distribution model of piezoelectric materials (Fig. 8). For the wurtzite structure of ZnO in piezoelectric phase, there is no internal dipole with the positive and negative charges of the whole system coincident without strain (Fig. 8a). When subjected to strain, dipole moments are yielded by the lattice displacement of ZnO while compressive and tensile stress produce the polarized electric field in various directions as demonstrated in Figs. 8b and8c, respectively. Driven by such polarization potential, the free charges are separated and forced to move to opposite directions resulting in the inhibition of recombination of charge carriers, and thus more holes and electrons arrive at the active site for catalytic redox reactions. What's more, the spatial separation of charge carriers reduces not only the recombination of electron-hole pairs, but also the probability of reverse reactions between oxidation products and reduction products.

In this work, piezoelectric polarization and its effect on adsorption behavior and catalytic reaction of HCHO oxidation were explored. As shown in Fig. 8d, the piezoelectric effect enhances the adsorption of HCHO and O_2 onto ZnO surface, which could be contributed to piezoelectric materials being able to collect external vibration energy and releasing a large number of free charges to participate in piezopotentail catalytic reaction. Without strain, O-O bond breaking in *OOH species is the rate determining step with a high barrier of 1.29 eV (step 2) in the entire reaction onto ZnO(100), while such barrier is greatly reduced to 0.14 eV by piezoelectric polarization induced by external force. Interestingly, in −12 % ZnO(100) system, the rate determining step of entire reaction is HCO_2* dehydrogenation with a free energy barrier of 0.79 eV, which is much lower than the rate determining step energy barrier of 1.29 eV in 0 % ZnO(100) system. The results not only

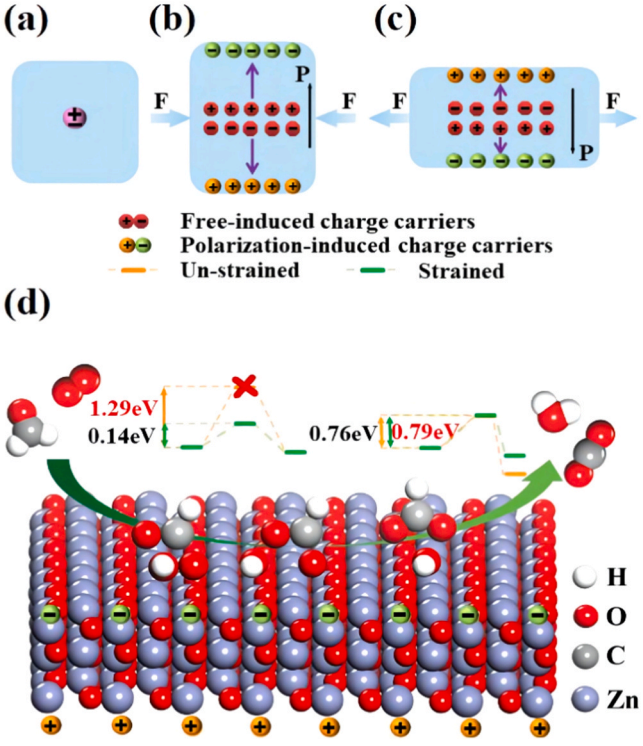

Fig. 8. Piezoelectric materials (a) without strain, (b) under compression, and (c) under tension; (d) piezoelectric catalytic oxidation mechanism of HCHO onto compressive strained ZnO surface.

rationalize the enhanced activity of piezoelectric potential for catalytic oxidation of HCHO onto ZnO surface from the atomic level, but also resolve the catalyst deactivation problem by easily desorb the formed products CO_2 and H_2O molecules from ZnO surface, which also provides theoretical guidance for experimental development of environmentally friendly piezoelectric catalysis.

4. Conclusions

In the present work, DFT calculations were conducted to systematically study piezoelectric catalytic oxidation of HCHO onto ZnO(100) under a series of strain ratios. The atomic and adsorption changes were initially studied during piezoelectric process. In accordance with trends of structural change, we found that the compressive strain would yield stronger adsorption free energy for both HCHO and O_2 species onto ZnO (100), while tensile force has little effect on adsorption. Additionally, the relationship between external strain intensity, electronic structure and adsorption energy was constructed further to evaluate the optimal strain intensity range for the catalytic effect, which are also verified by the calculated total density of states, Bader charge and charge density difference analysis. Then, HCHO oxidation begins with co-adsorption of HCHO and O_2 adsorbed onto ZnO(100) surface through the Langmuir Hinshelwood mechanism. Unexpectedly, piezoelectric polarization induced by external force can greatly reduce the free energy barrier and alter the rate-determining step in catalytic oxidation of HCHO by LH mechanism. We found that the free energy barrier for the rate determining step (O-O bond breaking of *OOH species) is significantly reduced from 1.29 to 0.14 eV onto ZnO(100) under compression strain of −12 %, making HCO_2* dehydrogenation as new rate-determining step with a free energy barrier of 0.79 eV. The origin of the improved piezopotentail catalytic activity could be contributed to the effectively separated intrinsic free charges by a built-in electric field (pizeopotential) in piezoelectric crystallites emerging as the role of charge transfer in the catalysis process via regulating the concentration of free charge carriers. That is, the application of piezoelectric potential not only enhanced the catalytic oxidation activity of HCHO onto ZnO surface, but also resolved the catalyst deactivation problem by easily desorb CO_2 and H_2O molecules from ZnO surface. This study can provide theoretical guidance towards the advancement of piezocatalysis design for pollutant degradation.

CRediT authorship contribution statement

Weina Zhao: Writing – original draft, Methodology, Investigation. **Guiying Li:** Writing – review & editing. **Gu Wang:** Methodology, Investigation, Formal analysis, Data curation. **Taicheng An:** Writing – review & editing, Supervision. **Shengnan Song:** Investigation. **Meicheng Wen:** Methodology.

Declaration of Competing Interest

The authors declare that they have no known competing financial interests or personal relationships that could have appeared to influence the work reported in this paper.

Data availability

No data was used for the research described in the article.

Acknowledgments

This work was supported by the National Natural Science Foundation of China (22006023), Guangdong Provincial Key R&D Program (2022-GDUT-A0007), Natural Science Foundation of Guangdong Province (2019A1515010428) and Guangzhou Science and Technology Project (202102020126).

Appendix A. Supporting information

Supplementary data associated with this article can be found in the online version at doi:10.1016/j.apcatb.2024.124057.

References

[1] Z. Li, R. Gao, Z. Hou, X. Yu, H. Dai, J. Deng, Y. Liu, Tandem supported Pt and ZSM-5 catalyst with separated catalytic functions for promoting multicomponent VOCs oxidation, Appl. Catal. B Environ. 339 (2023) 123131.
[2] C. He, J. Cheng, X. Zhang, M. Douthwaite, S. Pattisson, Z. Hao, Recent advances in the catalytic oxidation of volatile organic compounds: a review based on pollutant sorts and sources, Chem. Rev. 119 (2019) 4471–4568.
[3] National criteria of the People's Republic of China, GB/T 50325-2010, Criterion for controlling the indoor air pollutant in civil architecture projects (in Chinese).
[4] S. Brosillon, M.-H. Manero, J.-N. Foussard, Mass Transfer in VOC adsorption on zeolite: experimental and theoretical breakthrough curves, Environ. Sci. Technol. 35 (2001) 3571–3575.
[5] X. Li, Y. Sun, T. Zhang, Y. Bai, X. Lyu, W. Cai, Y. Li, N-doping nanoporous carbon microspheres derived from MOFs for highly efficient removal of formaldehyde, Nanotechnology 30 (2019) 105702.
[6] F. Liu, S. Rong, P. Zhang, L. Gao, One-step synthesis of nanocarbon-decorated MnO_2 with superior activity for indoor formaldehyde removal at room temperature, Appl. Catal. B Environ. 235 (2018) 158–167.
[7] J. Deng, W. Song, L. Chen, L. Wang, M. Jing, Y. Ren, Z. Zhao, J. Liu, The effect of oxygen vacancies and water on HCHO catalytic oxidation over Co_3O_4 catalyst: a combination of density functional theory and microkinetic study, Chem. Eng. J. 355 (2019) 540–550.
[8] J. Yu, X. Li, Z. Xu, W. Xiao, NaOH-Modified ceramic honeycomb with enhanced formaldehyde adsorption and removal performance, Environ. Sci. Technol. 47 (2013) 9928–9933.
[9] H. Wu, S. Ma, W. Song, E.J.M. Hensen, Density functional theory study of the mechanism of formaldehyde oxidation on Mn-Doped Ceria, J. Phys. Chem. C. 120 (2016) 13071–13077.
[10] C. Wang, Y. Li, C. Zhang, X. Chen, C. Liu, W. Weng, W. Shan, H. He, A simple strategy to improve Pd dispersion and enhance Pd/TiO_2 catalytic activity for formaldehyde oxidation: the roles of surface defects, Appl. Catal. B Environ. 282 (2021) 119540.
[11] Y. Chen, G. Jiang, X. Cui, Z. Zhang, X. Hou, Fabrication of Pd/CeO_2 nanocubes as highly efficient catalysts for degradation of formaldehyde at room temperature, Catal. Sci. Technol. 11 (2021) 6732–6741.
[12] B. Chen, Q. Zhao, L. Yu, L. Chen, M. Crocker, C. Shi, New insights into the size and support effects of γ-Al_2O_3 supported Au catalysts for HCHO oxidation at room temperature, Catal. Sci. Technol. 10 (2020) 4571–4579.
[13] X. Qin, X. Chen, M. Chen, J. Zhang, H. He, C. Zhang, Highly efficient Ru/CeO_2 catalysts for formaldehyde oxidation at low temperature and the mechanistic study, Catal. Sci. Technol. 11 (2021) 1914–1921.
[14] Q. Li, J. Zhou, D. Li, Z. Ao, Understanding the structure–activity relationships of different double atom catalysts from density functional calculations: three general rules for efficient CO oxidation, J. Mater. Chem. A 10 (2022) 9025–9036.
[15] F. Jiang, Z. Zhou, C. Zhang, C. Feng, G. Xiong, Y. Wang, Z. Fei, Y. Liu, Y. Pan, Structural regulation of single-atom catalysts for enhanced catalytic oxidation performance of volatile organic compounds, Nano Res. 16 (2023) 1967–1983.
[16] W. Han, W. Ling, P. Gao, F. Dong, Z. Tang, Engineering Pt single atom catalyst with abundant lattice oxygen by dual nanospace confinement strategy for the efficient catalytic elimination of VOCs, Appl. Catal. B Environ. 345 (2024) 123687.
[17] A. Zhang, Z. Liu, B. Xie, J. Lu, K. Guo, S. Ke, L. Shu, H. Fan, Vibration catalysis of eco-friendly $Na_{0.5}K_{0.5}NbO_3$-based piezoelectric: an efficient phase boundary catalyst, Appl. Catal. B Environ. 279 (2020) 119353.
[18] J. Wang, X. Zhou, J. Hao, Z. Wang, B. Huo, J. Qi, Y. Wang, F. Meng, Sustainable self-powered degradation of antibiotics using Fe_3O_4@MoS_2/PVDF modified pipe with superior piezoelectric activity: mechanism insight, toxicity assessment and energy consumption, Appl. Catal. B Environ. 331 (2023) 122655.
[19] J. Wu, N. Qin, D. Bao, Effective enhancement of piezocatalytic activity of $BaTiO_3$ nanowires under ultrasonic vibration, Nano Energy 45 (2018) 44–51.
[20] H. Li, W. Ma, X. Zeng, S. Liu, L. Xiao, Z. Fang, Y. Feng, M. Yang, H. Zhu, Y. Yang, H. Liu, ZnO/CuO Piezoelectric nanocatalysts for the degradation of organic pollutants, ACS Appl. Nano Mater. 6 (2023) 21113–21122.
[21] J. Chen, B. Liao, X. Liao, H. Xie, Y. Yu, S. Hou, C. Wang, X. Fan, Strain-driven polarized electric field-promoted photocatalytic activity in borate-based $CsCdBO_3$ bulk materials, ACS Appl. Mater. Interfaces 13 (2021) 34202–34212.
[22] J. Shi, S. Yang, Z. Zheng, J. Li, L. Wang, W. Zeng, L. Yang, Y. Xiong, Z. Jin, X. Tao, Textile-based piezocatalytic platform for organics degradation under low-frequency water flow, J. Mater. Chem. A 11 (2023) 7596–7604.
[23] H. Zheng, Y. Wang, J. Liu, J. Wang, K. Yan, K. Zhu, Recent advancements in the use of novel piezoelectric materials for piezocatalytic and piezo-photocatalytic applications, Appl. Catal. B Environ. 341 (2024) 123335.
[24] Y. Zhu, W. Zhao, B. Jing, J. Zhou, B. Cai, D. Li, Z. Ao, Density functional theory calculations on 2H-MoS_2 monolayer for HCHO degradation: Piezoelectric-photocatalytic synergy, Chin. Chem. Lett. 34 (2023) 107816.
[25] Z. Liang, C.-F. Yan, S. Rtimi, J. Bandara, Piezoelectric materials for catalytic/photocatalytic removal of pollutants: Recent advances and outlook, Appl. Catal. B Environ. 241 (2019) 256–269.

[26] V.A. Cao, M. Kim, S. Lee, C.G. Kim, P. Cao Van, T.N. Thi, J.-R. Jeong, J. Nah, Enhanced output performance of a flexible piezoelectric nanogenerator realized by lithium-doped zinc oxide nanowires decorated on MXene, ACS Appl. Mater. Interfaces 14 (2022) 26824–26832.
[27] Y. Zhang, C. Liu, J. Liu, J. Xiong, J. Liu, K. Zhang, Y. Liu, M. Peng, A. Yu, A. Zhang, Y. Zhang, Z. Wang, J. Zhai, Z.L. Wang, Lattice strain induced remarkable enhancement in piezoelectric performance of ZnO-based flexible nanogenerators, ACS Appl. Mater. Interfaces 8 (2016) 1381–1387.
[28] Y. Zhang, H. Jang, X. Ge, W. Zhang, Z. Li, L. Hou, L. Zhai, X. Wei, Z. Wang, M. G. Kim, S. Liu, Q. Qin, X. Liu, J. Cho, Single-Atom Sn on Tensile-Strained ZnO Nanosheets for Highly Efficient Conversion of CO_2 into Formate, Adv. Energy Mater. 12 (2022) 2202695.
[29] H. You, Z. Wu, L. Zhang, Y. Ying, Y. Liu, L. Fei, X. Chen, Y. Jia, Y. Wang, F. Wang, S. Ju, J. Qiao, C. Lam, H. Huang, Harvesting the vibration energy of $BiFeO_3$ nanosheets for hydrogen evolution, Angew. Chem. Int. Ed. 58 (2019) 11779–11784.
[30] Y.-L. Liu, J.M. Wu, Synergistically catalytic activities of $BiFeO_3/TiO_2$ core-shell nanocomposites for degradation of organic dye molecule through piezophototronic effect, Nano Energy 56 (2019) 74–81.
[31] J. Wu, N. Qin, B. Yuan, E. Lin, D. Bao, Enhanced pyroelectric catalysis of $BaTiO_3$ nanowires for utilizing waste heat in pollution treatment, ACS Appl. Mater. Interfaces 10 (2018) 37963–37973.
[32] J. Wu, Q. Xu, E. Lin, B. Yuan, N. Qin, S.K. Thatikonda, D. Bao, Insights into the Role of Ferroelectric Polarization in Piezocatalysis of Nanocrystalline $BaTiO_3$, ACS Appl. Mater. Interfaces 10 (2018) 17842–17849.
[33] F. Opoku, P.P. Govender, Highly Selective and Sensitive detection of Formaldehyde by β_{12} -Borophene/SnO_2 Heterostructures: the role of an external electric field and in-plain biaxial strain, J. Phys. Chem. A 124 (2020) 2288–2300.
[34] J.M. Wu, W.E. Chang, Y.T. Chang, C. Chang, Piezo-catalytic effect on the enhancement of the ultra-high degradation activity in the dark by single- and few-layers MoS_2 nanoflowers, Adv. Mater. 28 (2016) 3718–3725.
[35] S. Li, Z. Zhao, D. Yu, J.-Z. Zhao, Y. Su, Y. Liu, Y. Lin, W. Liu, H. Xu, Z. Zhang, Few-layer transition metal dichalcogenides (MoS_2, WS_2, and WSe_2) for water splitting and degradation of organic pollutants: understanding the piezocatalytic effect, Nano Energy 66 (2019) 104083.
[36] W. Wu, L. Wang, Y. Li, F. Zhang, L. Lin, S. Niu, D. Chenet, X. Zhang, Y. Hao, T. F. Heinz, J. Hone, Z.L. Wang, Piezoelectricity of single-atomic-layer MoS_2 for energy conversion and piezotronics, Nature 514 (2014) 470–474.
[37] Z.L. Wang, Nanostructures of zinc oxide, Mater. Today 7 (2004) 26–33.
[38] Z.L. Wang, J. Song, Piezoelectric nanogenerators based on zinc oxide nanowire arrays, Science 312 (2006) 242–246.
[39] Y. Wen, J. Chen, X. Gao, W. Liu, H. Che, B. Liu, Y. Ao, Two birds with one stone: Cobalt-doping induces to enhanced piezoelectric property and persulfate activation ability of ZnO nanorods for efficient water purification, Nano Energy 107 (2023) 108173.
[40] Z. Kang, H. Si, S. Zhang, J. Wu, Y. Sun, Q. Liao, Z. Zhang, Y. Zhang, Interface engineering for modulation of charge carrier behavior in ZnO photoelectrochemical water splitting, Adv. Funct. Mater. 29 (2019) 1808032.
[41] L. Jing, Y. Xu, M. Xie, Z. Li, C. Wu, H. Zhao, J. Wang, H. Wang, Y. Yan, N. Zhong, H. Li, J. Hu, Piezo-photocatalysts in the field of energy and environment: designs, applications, and prospects, Nano Energy 112 (2023) 108508.
[42] D. Masekela, N.C. Hintsho-Mbita, S. Sam, T.L. Yusuf, N. Mabuba, Application of $BaTiO_3$-based catalysts for piezocatalytic, photocatalytic and piezo-photocatalytic degradation of organic pollutants and bacterial disinfection in wastewater: a comprehensive review, Arab. J. Chem. 16 (2023) 104473.
[43] X. Yang, J. Wang, A.M. El-Sherbeeny, A.A. AlHammadi, W.-H. Park, M. R. Abukhadra, Insight into the adsorption and oxidation activity of a ZnO/ piezoelectric quartz core-shell for enhanced decontamination of ibuprofen: Steric, energetic, and oxidation studies, Chem. Eng. J. 431 (2022) 134312.
[44] W. Ma, M. Lv, F. Cao, Z. Fang, Y. Feng, G. Zhang, Y. Yang, H. Liu, Synthesis and characterization of ZnO-GO composites with their piezoelectric catalytic and antibacterial properties, J. Environ. Chem. Eng. 10 (2022) 107840.
[45] M. Zhang, H. Tao, C. Zhai, J. Yang, Y. Zhou, D. Xia, G. Comodi, M. Zhu, Twin-brush ZnO mesocrystal for the piezo-activation of peroxymonosulfate to remove ibuprofen in water: performance and mechanism, Appl. Catal. B Environ. 326 (2023) 122399.
[46] C. Wang, C. Hu, F. Chen, T. Ma, Y. Zhang, H. Huang, Design strategies and effect comparisons toward efficient piezocatalytic system, Nano Energy 107 (2023) 108093.
[47] M. Catti, Y. Noel, R. Dovesi, Full piezoelectric tensors of wurtzite and zinc blende ZnO and ZnS by first-principles calculations, J. Phys. Chem. Solids 64 (2003) 2183–2190.
[48] J. Heyd, G.E. Scuseria, M. Ernzerhof, Hybrid functionals based on a screened Coulomb potential, J. Chem. Phys. 118 (2003) 8207–8215.
[49] G. Henkelman, A. Arnaldsson, H. Jónsson, A fast and robust algorithm for Bader decomposition of charge density, Comput. Mater. Sci. 36 (2006) 354–360.
[50] V. Wang, N. Xu, J.-C. Liu, G. Tang, W.-T. Geng, VASPKIT: a user-friendly interface facilitating high-throughput computing and analysis using VASP code, Comput. Phys. Commun. 267 (2021) 108033.
[51] G. Henkelman, H. Jónsson, A climbing image nudged elastic band method for finding saddle points and minimum energy paths, J. Chem. Phys. 113 (2000) 9901–9904.
[52] Ü. Özgür, I. Ya, C. Alivov, A. Liu, M.A. Teke, S. Reshchikov, V. Doğan, S.-J. Avrutin, H. Cho, A. Morkoç, comprehensive review of ZnO materials and devices, J. Appl. Phys. 98 (2005) 041301.
[53] Q. Liu, W. Zhao, Z. Ao, T. An, Photo-piezoelectric synergistic degradation of typical volatile organic compounds on BaTiO3, Chin. Chem. Lett. 33 (2022) 410–414.
[54] J.B. Neaton, C. Ederer, U.V. Waghmare, N.A. Spaldin, K.M. Rabe, First-principles study of spontaneous polarization in multiferroic $BiFeO_3$, Phys. Rev. B 71 (2005) 014113.
[55] Y. Zhao, Z. Zhang, C. Yang, H. Fan, J. Wang, Z. Tian, H. Zhang, Critical role of water on the surface of ZnO in H_2S removal at room Temperature, Ind. Eng. Chem. Res. 57 (2018) 15366–15374.
[56] M. Catti, Y. Noel, R. Dovesi, Full piezoelectric tensors of wurtzite and zinc blende ZnO and ZnS by first-principles calculations, J. Phys. Chem. Solids 64 (2003) 2183–2190.
[57] S. Holdren, R. Tsyshevsky, K. Fears, J. Owrutsky, T. Wu, X. Wang, B.W. Eichhorn, M.M. Kuklja, M.R. Zachariah, Adsorption and destruction of the G-Series nerve agent simulant dimethyl methylphosphonate on zinc oxide, ACS Catal. 9 (2019) 902–911.
[58] M. Wang, W. Wang, M. Ji, X. Cheng, Adsorption of phenol and hydrazine upon pristine and X-decorated (X = Ti, Cr and Mn) MoS_2 monolayer, Appl. Surf. Sci. 439 (2018) 350–363.
[59] H.V. Thang, S. Tosoni, G. Pacchioni, Evidence of charge transfer to atomic and molecular adsorbates on ZnO/X(111) (X = Cu, Ag, Au) ultrathin films. relevance for Cu/ZnO catalysts, ACS Catal. 8 (2018) 4110–4119.
[60] J. Ding, Y. Yang, J. Liu, Z. Wang, Catalytic reaction mechanism of formaldehyde oxidation by oxygen species over Pt/TiO_2 catalyst, Chemosphere 248 (2020) 125980.
[61] J. Zhou, G. Liu, Q. Jiang, W. Zhao, Z. Ao, T. An, Density functional theory calculations on single atomic catalysis: Ti-decorated $Ti_3C_2O_2$ monolayer (MXene) for HCHO oxidation, Chin. J. Catal. 41 (2020) 1633–1644.
[62] Q. Jiang, Z. Ao, S. Li, Z. Wen, Density functional theory calculations on the CO catalytic oxidation on Al-embedded graphene, RSC Adv. 4 (2014) 20290–20296.
[63] Y. Sekine, Oxidative decomposition of formaldehyde by metal oxides at room temperature, Atmos. Environ. 36 (2002) 5543–5547.